Research Square

Preprints are preliminary reports that have not undergone peer review.
They should not be considered conclusive, used to inform clinical practice,
or referenced by the media as validated information.

Chirality routing non-polaritonic vacuum correlations in Landau polaritons

Dukhyung Lee

Dukhyung.LEE@um6p.ma

Mohammed VI Polytechnic University https://orcid.org/0000-0003-1878-175X

Ayoub EL-Amrani

Mohammed VI Polytechnic University

Zakaria Mzaouali

Forschungszentrum Jülich GmbH

Houssam Sabri

University of New Hampshire https://orcid.org/0000-0002-1639-1566

abdelouahad el fatimy

Mohammed VI Polytechnic University https://orcid.org/0000-0001-6500-7762

Herschel Rabitz

Princeton University https://orcid.org/0000-0002-4433-6142

Article

Keywords:

Posted Date: June 12th, 2026

DOI: https://doi.org/10.21203/rs.3.rs-9889704/v1

License: This work is licensed under a Creative Commons Attribution 4.0 International License.
Read Full License

Additional Declarations: There is **NO** Competing Interest.

Chirality routing non-polaritonic vacuum correlations in Landau polaritons

Ayoub El-Amrani,[1,*] Zakaria Mzaouali,[2,3] Houssam Sabri,[1]
Herschel Rabitz,[4] Abdelouahed El Fatimy,[1] and Dukhyung Lee[1,†]

[1]*College of Physical Sciences and Engineering, University Mohammed VI Polytechnic, Ben Guerir, 43150, Morocco.*
[2]*Jülich Supercomputing Centre, Institute for Advanced Simulation, Forschungszentrum Jülich, Wilhelm-Johnen-Straße, Jülich, 52428, Germany.*
[3]*Institut für Theoretische Physik, Universität Tübingen, Auf der Morgenstelle 14, 72076 Tübingen, Germany.*
[4]*Department of Chemistry, Princeton University, Princeton, New Jersey 08544, USA.*

Ultrastrong coupling between matter and cavity vacuum fields can turn the electromagnetic vacuum into a structured quantum environment, thereby opening passive routes for modifying and manipulating material properties. Recent work has identified light–matter entanglement as an important ingredient in these property changes, which raises the question of where the relevant vacuum correlations actually reside. Landau polaritons provide chiral ultrastrong coupling systems in which one circular cavity polarization forms the bright polariton branches. Here, using a quantum information approach, we show that an exact chiral charge in a multimode Hopfield model routes the dominant anomalous correlations, squeezing, and cavity–matter entanglement into the opposite polarization. We find that, using parameters extracted from a multimode Landau polariton system, this hidden sector correlates the cyclotron resonance with finite momentum magnetoplasmons through Gaussian discord, while pairwise matter–matter entanglement remains absent. We further predict a polarization anisotropy of dressed vacuum electric field fluctuations as a signature of this chiral routing. These results identify chirality as a symmetry principle for organizing ultrastrong coupling vacua and show that quantum information tools provide a powerful framework for revealing the salient properties of Landau polaritons.

INTRODUCTION

Ultrastrong light–matter coupling (USC) profoundly reshapes the quantum vacuum of cavity systems. When the interaction energy becomes comparable to the bare frequencies of the uncoupled subsystems, the rotating wave approximation breaks down, and both counter-rotating and diamagnetic terms become essential ingredients of the theory [1–3]. In this regime, photonic and material excitations hybridize non-perturbatively into polaritonic normal modes [4], while the ground state is converted from an empty vacuum into a dressed Gaussian state hosting squeezed fluctuations and anomalous correlations [1, 5, 6]. Although these vacuum fluctuations do not appear as real photon populations in equilibrium [5], they lead to solid physical impacts: response functions, spectral properties, and other measurable observables can be modified without requiring the extraction of real photons [6–9]. Direct access to such vacuum excitations can be implemented through dedicated probing protocols, including non-adiabatic modulation, spontaneous conversion schemes, electroluminescence proposals, and coherent transfer or open system detection strategies [10–15].

In solid state platforms, the physical consequences of the vacuum become particularly evident. In Landau polariton systems, cavity vacuum fields have been shown to modify the transport and collective properties of a two-dimensional electron gas (2DEG) in equilibrium [16–18]. More directly, vacuum field correlations can now be accessed through field correlation measurements without relying on photon emission or population extraction [19]. These developments establish USC ground states as structured quantum environments with observable consequences, motivating a question: how are the quantum correlations and field fluctuations of the dressed vacuum distributed among the underlying light and matter modes?

Landau polaritons provide a particularly rich setting for this question. A 2DEG subjected to a perpendicular magnetic field (c.f. Fig. 1b) supports cyclotron and magnetoplasmon excitations that can couple to terahertz cavity modes, reaching the ultrastrong and even deep strong coupling regimes [20–23]. Because several collective electronic modes can couple to the same cavity resonance, the platform naturally realizes a multimode light–matter problem beyond the minimal case of a single light-matter pair. Recent works have experimentally demonstrated the multimode polaritonic spectrum, whose mode structure is accurately described by Hopfield-type models [23, 24]. This raises a question that is complementary to spectroscopy: is cavity mediation in the ultrastrong coupling vacuum exhausted by the hybridization visible in the polariton spectrum, or does it also redistribute quantum correlations between local and nonlocal electronic modes?

More broadly, chiral light–matter interactions have become an increasingly active frontier across nanophotonics, condensed matter cavity QED, and quantum technologies, driven by the possibility of engineering chiral electromagnetic environments that control symmetry breaking, light, charge, and spin [25–28]. A key feature of the Landau polariton platform is its intrinsic chirality. In a circular polarization basis, only one cavity polarization mode couples resonantly

to matter, whereas the complementary polarization enters only through counter-rotating processes [24, 29]. In spectroscopic language, one sector is active, hosting the familiar avoided crossing polariton branches, while the complementary inactive sector does not generate the conventional polariton anticrossings, instead appearing through the vacuum Bloch–Siegert shift [29]. What has remained unclear, however, is whether the same active/inactive separation also governs the equilibrium quantum vacuum, or whether it is only a feature of the spectroscopic branches.

Here we show that this polarization asymmetry originates from the structure of the Hopfield Hamiltonian. We identify a conserved chiral $U(1)$ charge that imposes strict selection rules on anomalous correlators and therefore fixes the allowed symmetry channels through which ground state squeezing and entanglement can be distributed. The symmetry suppresses anomalous channels involving the spectroscopically active polarization while leaving the complementary counter-rotating channel symmetry allowed, as summarized in Fig. 1a. The resulting vacuum structure is therefore *non-polaritonic* in an operational sense: its dominant correlations are organized not by the active polarization that forms the observed polariton branches, but by the orthogonal counter-rotating sector of the same Hopfield Hamiltonian. We then investigate how this symmetry is realized in an experimentally verified model system of a multimode Landau polariton Hamiltonian using continuous variable quantum information diagnostics [30–36]. This approach have played an important role in revealing correlation structures that are not directly visible in conventional observables [37–46]. Here we use the same philosophy in a bosonic light–matter vacuum to show how the dressed ground state is correlated in the underlying cavity and collective electronic degrees of freedom. Since the Hamiltonian is quadratic, this information is fully encoded in the Gaussian covariance matrix, allowing vacuum fluctuations, logarithmic negativity, Gaussian discord, and graph state nullifiers to identify the entangling channels, the nonclassical matter correlations, and the organized multimode squeezing of the ultrastrong coupling vacuum [36, 47, 48]. In this sense, the quantum information measures act as a probe of the symmetry organized vacuum structure of Landau polaritons. Recent driven dissipative work also identified light–matter entanglement and quadrature squeezing as characteristic observables of Landau polariton dynamics [49], further supporting the use of quantum information diagnostics in this platform.

Using this approach, we find that the polarization dominating the polariton spectrum remains essentially separable from the electronic modes in equilibrium, whereas the orthogonal polarization acts as the main mediator of vacuum squeezing and quantum correlations. In this sense, the dominant vacuum structure is non-polaritonic: it is organized by the polarization sector that does not form the bright polariton branches. We further show that the cavity-mediated coupling between local and nonlocal matter modes appears in the equilibrium vacuum predominantly as Gaussian discord without detectable pairwise matter–matter entanglement. In other words, the cavity mediates genuinely nonclassical, yet non-entangling, correlations inside the matter sector: quantum correlations that cannot be reduced to locally accessible classical information, even though they do not take the form of pairwise entanglement. This redistribution is routed predominantly through the complementary counter-rotating polarization and, for the experimentally extracted parameter set, gives rise to a nearly pure, genuinely multipartite correlated subsystem consistent with a star-like Gaussian graph state interpretation (Fig. 1c).

Finally, we translate the chiral routing into a field level signature. Because the two circular cavity modes are dressed unequally, the vacuum electric field fluctuations become anisotropic in polarization space. This polarization-resolved fluctuation anisotropy provides an observable fingerprint of the hidden non-polaritonic vacuum structure: the symmetry-selected redistribution of vacuum correlations enhances or suppresses field noise depending on the polarization.

Our findings elevate the polarization asymmetry of Landau polaritons from a spectroscopic observation to a symmetry principle governing the ultrastrong coupling vacuum. While the underlying polarization asymmetric Hamiltonian can be inferred from the polariton spectrum, the vacuum correlations themselves remain hidden from conventional spectroscopy. The chiral selection rule and quantum information diagnostics reveal where the equilibrium vacuum correlations actually reside, information that is not directly readable from the spectroscopic dispersion alone. This hidden organization may be probed through vacuum field correlation measurements and may manifest in polarization sensitive response and magnetotransport in cavity coupled electron systems [16–19, 29, 50].

RESULTS

Chiral symmetry selection rules for the vacuum correlation channel. The central analytical result of this work is that the polarization-resolved Hopfield Hamiltonian possesses an exact chiral symmetry that already distinguishes the sector hosting the polariton branches from the sector carrying anomalous vacuum correlations. Related chiral light–matter physics beyond the rotating wave approximation has been investigated previously in a two-mode chiral Rabi model, where a copolarized mode couples through rotating wave terms while a counter-polarized mode is activated through counter-rotating processes under a conserved $U(1)$ quantity associated with angular momentum [51]. Much more abundant physics exists in Landau polariton systems: here the same chiral logic is realized in a solid state cavity QED platform described

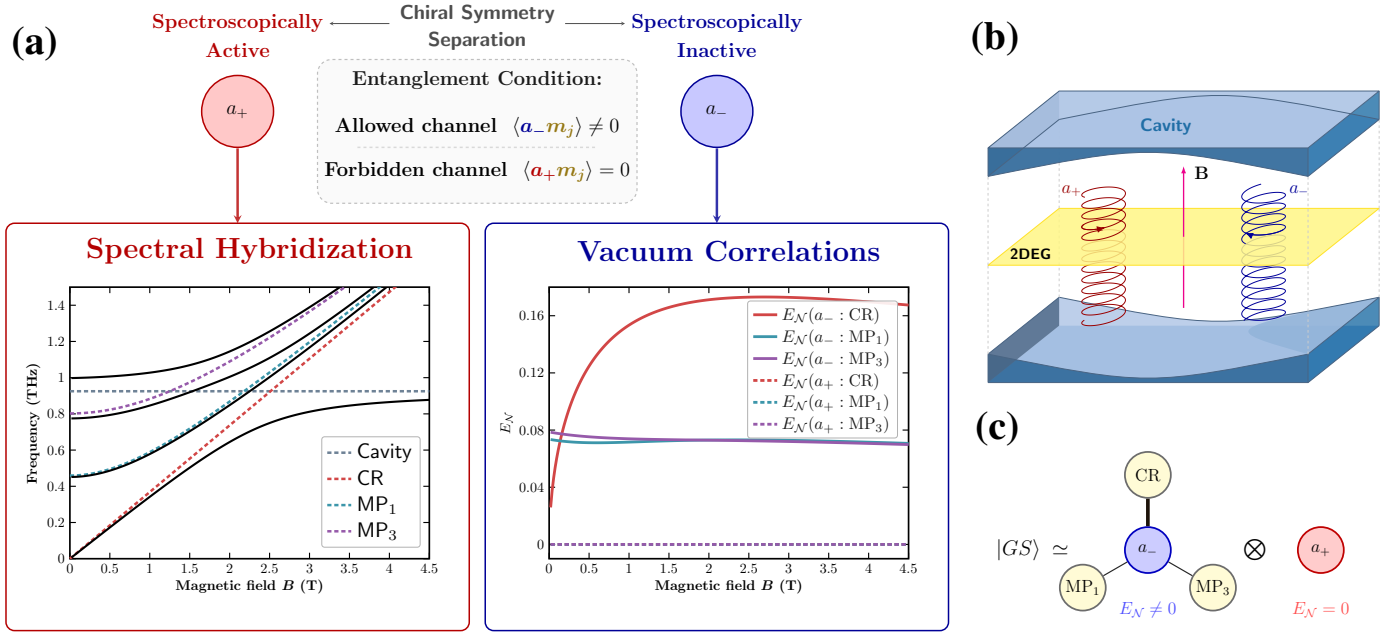


FIG. 1: Chiral symmetry separating the bright polariton sector from vacuum correlation channels. **(a)** Structure of the multimode Landau polariton Hamiltonian, Eq. (1). The circular polarization a_+ is spectroscopically active and organizes the bright polariton hybridization, while the orthogonal polarization a_- hosts the anomalous vacuum correlation channels allowed by the symmetry. The chiral symmetry forbids anomalous a_+-matter correlations, $\langle a_+ m_j \rangle = 0$, while allowing the corresponding a_--matter channels, $\langle a_- m_j \rangle \neq 0$. The spectral hybridization and the vacuum correlations quantified by logarithmic negativity $E_{\mathcal{N}}$, Eq. 29 of Supplementary Note 5, were calculated based on the model system suggested in Fig. 2a. **(b)** Schematic diagram of a Landau polariton system coupled with an optical cavity: a two-dimensional electron gas (2DEG) embedded in a terahertz cavity under a perpendicular magnetic field, supporting cyclotron and finite momentum magnetoplasmon excitations. **(c)** Ground state correlation structure revealed in this work. The correlated sector is centered on a_-, with the strongest graph-like connection to the cyclotron mode, whereas a_+ remains nearly separable.

by a multimode Hopfield Hamiltonian, where the cavity couples not to a single two-level system but to collective bosonic excitations of a 2DEG, including both local and nonlocal modes, with the ability to continuously tune the interaction by a magnetic field. This makes it possible to address not only the chiral spectrum, but also how the symmetry reorganizes the equilibrium vacuum, rerouting squeezing and quantum correlations across the multimode matter sector. At the schematic level, the Hamiltonian can be written, in units of $\hbar = 1$, as

$$\begin{aligned} H &= \omega_0 \left(a_+^\dagger a_+ + a_-^\dagger a_- \right) + \sum_j \omega_j m_j^\dagger m_j \\ &+ i \sum_j g_j \left[m_j^\dagger (a_+ + a_-^\dagger) - m_j (a_- + a_+^\dagger) \right] \\ &+ D \, (a_- + a_+^\dagger)(a_+ + a_-^\dagger), \end{aligned} \tag{1}$$

where m_j denotes the collective matter modes.

A convenient way to expose the physical content of the Hamiltonian, Eq. (1), is to inspect the operator sectors closed under the Heisenberg equations. The dynamics separates into

$$\boldsymbol{\eta}_- = (a_+, m_1, m_2, \ldots, a_-^\dagger)^T, \tag{2}$$

$$\boldsymbol{\eta}_+ = (a_+^\dagger, m_1^\dagger, m_2^\dagger, \ldots, a_-)^T, \tag{3}$$

where the subscripts now follow the chiral charge of the sector. The active spectroscopic sector is therefore $\boldsymbol{\eta}_-$: it contains the cavity annihilation operator a_+ together with the matter annihilation operators m_j, i.e. the operators that can hybridize in the usual co-rotating, number conserving sense to form polaritonic normal modes. This is why the avoided crossing branches identified as polaritons live in the a_+ channel. By contrast, the inactive polarization enters the same sector only as the creation operator $a_-^\dagger$. It therefore does not participate in the usual spectroscopic hybridization, but instead appears through the antiresonant channel.

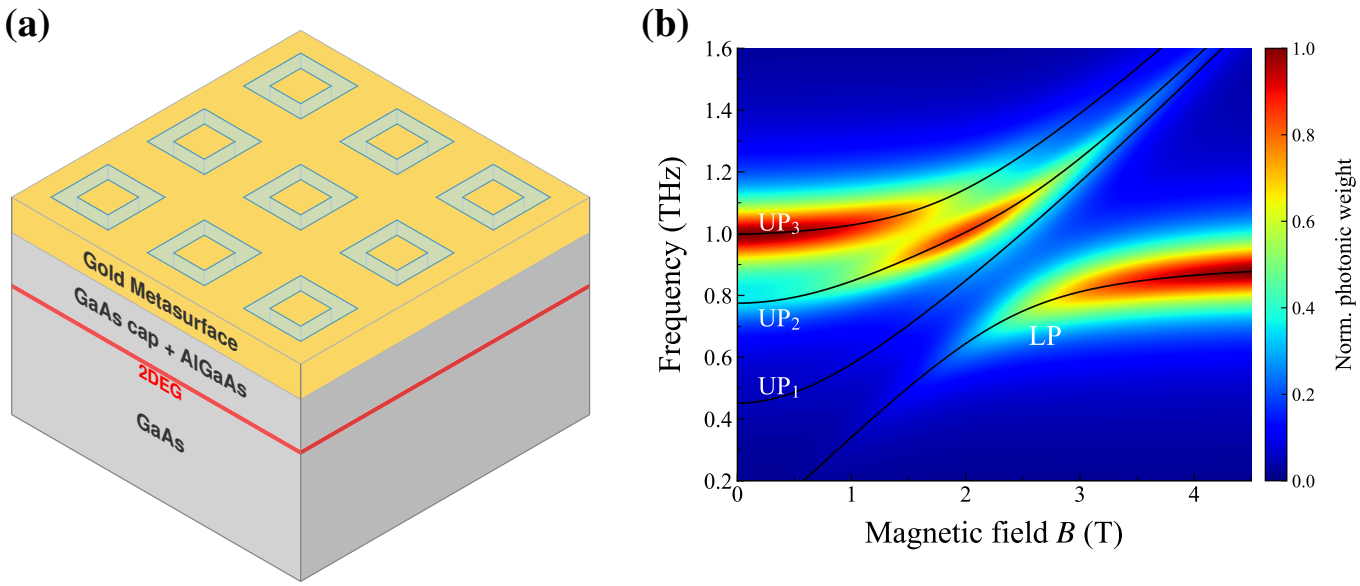


FIG. 2: Model system used in this work, previously demonstrated experimentally. **(a)** Schematic of the terahertz Landau polariton device: gold nanoslot cavities patterned above a GaAs/AlGaAs heterostructure hosting a 2DEG. **(b)** Lorentzian broadened photonic weight map for bright branches calculated from the multimode Hopfield model, reproducing the detected bright polariton branches. The map benchmarks the active spectroscopic sector.

This sector decomposition is the dynamical signature of the conserved chiral charge

$$Q = a_+^\dagger a_+ + \sum_j m_j^\dagger m_j - a_-^\dagger a_-, \qquad [H, Q] = 0. \tag{4}$$

Under the corresponding unitary transformation $U(\theta) = e^{-i\theta Q}$, the active polarization a_+ and the matter modes carry charge -1, while the inactive polarization a_- carries charge $+1$. As a consequence, any anomalous operator with nonzero Q charge has vanishing expectation value in a nondegenerate ground state. In particular,

$$\langle a_+ a_+ \rangle = 0, \qquad \langle a_+ m_j \rangle = 0, \tag{5}$$

for all matter modes m_j. The detailed derivation is given in Methods. A direct covariance matrix verification of the chiral selection rule is given in Supplementary Note 4.

Our key prediction is represented in Eq. (5), because the Hopfield Hamiltonian is quadratic in bosonic operators, its equilibrium ground state is Gaussian and is therefore fully characterized by second moments, including the anomalous pair correlators that encode vacuum squeezing and correlation structure [30]. In continuous variable Gaussian systems, squeezing is the nonclassical resource underlying Gaussian entanglement [52–54]. In the present quadratic ultrastrong coupling Hamiltonian, this squeezing originates from the anomalous correlations generated by the counter rotating sector [5]. The active polarization may therefore organize the polariton spectrum, but the vacuum squeezing and entangling channels are symmetry forbidden in that sector and remain allowed only through the inactive polarization a_-. The chiral symmetry therefore implies that the dominant ground state correlations reside not in the active spectroscopic channel, but in the inactive polarization sector.

The multimode model with a prior experimental demonstration. To test the symmetry prediction in a realistic setting, we use the multimode Landau polariton system of Ref. [24], whose polarization asymmetric Hamiltonian was experimentally inferred from transmission spectroscopy. The system consists of an array of gold slot cavities fabricated on a GaAs heterostructure hosting a high-mobility two-dimensional electron gas (2DEG), as sketched in Fig. 2a. The subwavelength confinement of the slot mode provides two essential ingredients: strong overlap between the THz near field and the 2DEG, and finite in-plane momentum components that allow the same cavity resonance to couple both to the local $k = 0$ cyclotron resonance (CR) and to finite-k magnetoplasmons. Such architectures build on the broader development of THz metamaterial and metasurface resonators, where strongly confined near fields enable ultrastrong light–matter coupling in deeply subwavelength mode volumes [20, 55, 56].

For the device parameters considered here, the bare cavity frequency is $\omega_0/2\pi \simeq 0.925$ THz. Among nonlocal modes, only modes with odd in-plane momentum components $k = n\pi/d$ ($n = 1, 3, \ldots$) are selectively excited due to the finite slot width $d = 4$ μm. The experimentally resolved multimode structure is captured by retaining the two lowest finite-k

components, MP_1 and MP_3, together with the CR. A perpendicular magnetic field tunes the matter spectrum through $\omega_c = eB/m^*$ where $m^* = 0.076\, m_0$ and

$$\omega^2_{\mathrm{MP},n}(B) = \omega^2_{p,n} + \omega^2_c(B), \tag{6}$$

producing distinct cavity detunings for CR, MP_1, and MP_3. The bare mode basis, active chiral block, and numerical parameter set used in these calculations are summarized in Supplementary Note 1. The normalized coupling strengths extracted from the measured branch positions are $g_{\mathrm{CR}}/\omega_0 \simeq 0.18$ for the CR channel and $g_1/\omega_0 \simeq g_3/\omega_0 \simeq 0.084$ for the magnetoplasmons. Thus the CR channel lies in the ultrastrong coupling regime, while the finite-k modes form a strongly coupled multimode sector.

The corresponding polarization-resolved multimode Hopfield Hamiltonian is now expanded with the cyclotron mode b and the magnetoplasmons c_n:

$$\begin{aligned} H = {} & \omega_0(a_+^\dagger a_+ + a_-^\dagger a_-) + \omega_c(B)\, b^\dagger b + \sum_{n=1,3} \omega_{\mathrm{MP},n}(B)\, c_n^\dagger c_n \\ & + i\Big[\Big(\bar{g}_{\mathrm{CR}}\, b^\dagger + \sum_{n=1,3} \bar{g}_n\, c_n^\dagger\Big)(a_+ + a_-^\dagger) \\ & - \Big(\bar{g}_{\mathrm{CR}}\, b + \sum_{n=1,3} \bar{g}_n\, c_n\Big)(a_- + a_+^\dagger)\Big] \\ & + D\,(a_- + a_+^\dagger)(a_+ + a_-^\dagger), \end{aligned} \tag{7}$$

with

$$\bar{g}_{\mathrm{CR}}(B) = g_{\mathrm{CR}}\sqrt{\frac{\omega_c(B)}{\omega_0}}, \qquad \bar{g}_n(B) = g_n\sqrt{\frac{\omega_{\mathrm{MP},n}(B)}{\omega_0}}, \tag{8}$$

and

$$D = \frac{\bar{g}^2_{\mathrm{CR}}}{\omega_c} + \sum_{n=1,3} \frac{\bar{g}_n^2}{\omega_{\mathrm{MP},n}}. \tag{9}$$

Figure 2b is the Lorentzian broadened photonic weight [5, 16] map as a spectroscopic benchmark for this model (as detailed in the Supplementary Note 3). The photonic weight map visualizing the active sector of the Hopfield Hamiltonian reproduces the experimentally observed branch pattern with the sequential avoided crossings. With this excellent agreement with the experimental spectrum established, we proceed to investigate the equilibrium vacuum correlations of the same Hamiltonian, using the chiral selection rule and quantum information diagnostics. If the symmetry prediction is correct, the polarization that organizes the observed anticrossings should remain weakly correlated with matter in the ground state, whereas the orthogonal counter-rotating polarization should carry the dominant squeezing and entanglement channels.

Vacuum entanglement routing through the inactive polarization. We quantified the degree of entanglement using the logarithmic negativity measure $E_{\mathcal{N}}$; the definitions and supporting photon–matter diagnostics are given in Supplementary Note 5. Figure 1a confirms the central symmetry prediction. Although the active polarization a_+ organizes the observed polariton anticrossings, its bipartite ground state entanglement with all matter excitations remains indistinguishable from zero within numerical precision over the entire magnetic field range. In contrast, the inactive polarization a_- exhibits finite logarithmic negativities with the CR and MP modes. That is,

$$E_{\mathcal{N}}(a_+ : \mathrm{CR}\ or\ \mathrm{MP}_1\ or\ \mathrm{MP}_3) = 0, \tag{10}$$

whereas

$$E_{\mathcal{N}}(a_- : \mathrm{CR}\ or\ \mathrm{MP}_1\ or\ \mathrm{MP}_3) > 0. \tag{11}$$

The quantum information analysis therefore verifies the symmetry-based prediction: while the active polarization a_+ remains effectively separable from the matter subsystem in the ground state, the inactive polarization a_- is precisely the channel through which entanglement and equilibrium squeezing are distributed.

Among the three inactive sector pairs, the strongest entanglement is found in the a_-–CR channel. It increases rapidly with magnetic field and reaches a broad maximum near the cyclotron zero detuning point. The correlations $E_{\mathcal{N}}(a_- : \mathrm{MP}_1)$ and $E_{\mathcal{N}}(a_- : \mathrm{MP}_3)$ are weaker and vary more gently with field, but remain clearly above zero across the investigated interval. This hierarchy reflects the coupling strengths and detunings in the system.

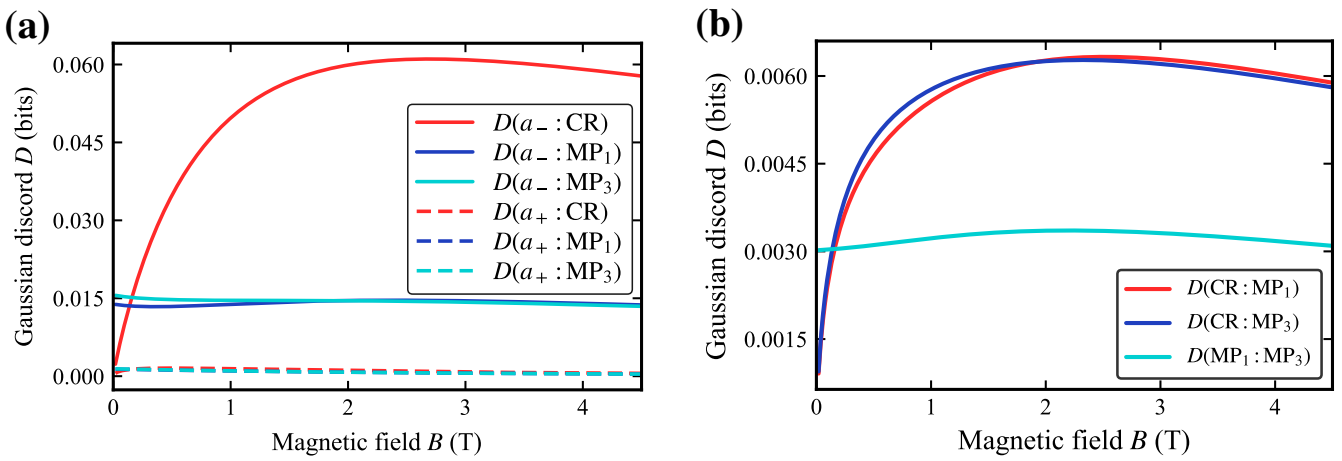


FIG. 3: Cavity-mediated nonclassical correlations in the vacuum graph state. (a) Gaussian discord between each cavity polarization and the matter modes as a function of magnetic field. The inactive polarization a_- develops substantially stronger nonclassical correlations with the cyclotron and magnetoplasmon modes than the spectroscopically active polarization a_+, in line with the trend observed in the logarithmic negativity $E_{\mathcal{N}}$. **(b)** Gaussian discord, between the matter modes. Although pairwise matter–matter entanglement vanishes throughout the field range, finite discord persists between the cyclotron and magnetoplasmon excitations. This shows that the hidden a_--centered vacuum sector leaves a nonclassical but non-entangling footprint inside the electronic subsystem. Gaussian discord is defined via Eq. 35 of Supplementary Note 5.

The low field limit further clarifies the origin of this behavior. As $B \to 0$, the cyclotron frequency $\omega_c = eB/m^*$ and the associated field-dependent coupling $\bar{g}_{\mathrm{CR}} \propto \sqrt{\omega_c/\omega_0}$ both vanish. Consequently, the entanglement $E_{\mathcal{N}}(a_- : \mathrm{CR})$ tends to zero in the same limit. The magnetoplasmon channels behave differently. Their frequencies satisfy

$$\omega^2_{\mathrm{MP},n}(B) = \omega^2_{p,n} + \omega^2_c(B), \tag{12}$$

so that, as the magnetic field is reduced, they continuously approach the underlying two-dimensional plasmon modes rather than disappearing. This difference is directly visible in the bare dispersions, shown as dashed lines in the left panel of Fig. 1a. Accordingly, the inactive sector entanglement involving MP_1 and MP_3 survives down to low magnetic fields, while the CR-related entanglement vanishes together with the cyclotron mode.

Cavity-mediated quantum correlations across local and nonlocal matter modes. The vanishing of bipartite entanglement between a_+ and the matter modes does not, by itself, exclude all quantum correlations in that sector. In general, entanglement does not represent all forms of quantumness: even in the absence of entanglement, separable states can still possess quantum correlations, captured quantum discord [57, 58]. For continuous variable Gaussian states, the corresponding measure is Gaussian discord [59, 60]. We therefore first examine whether the polarization hierarchy found from logarithmic negativity persists at the level of Gaussian discord. Because Gaussian discord depends on which subsystem is measured, we use its symmetrized form, as defined in Eq. 35 of Supplementary Note 5.

Figure 3a shows that the Gaussian discord follows the same hierarchy already observed in the logarithmic negativity. The symmetry selected a_- sector carries the dominant Gaussian discord with the matter modes, while the corresponding a_+–matter discord remains negligible. The strongest contribution again occurs in the a_-–CR channel, while the a_-–MP correlations are weaker but finite.

Having established that the relevant cavity channel for quantum correlations is a_-, we next ask what kind of correlations this hidden channel leaves inside the matter subsystem itself. There is growing interest in using cavity fields not only to hybridize individual excitations spectroscopically, but also to mediate effective interactions and correlations between distinct matter modes [61–64]. Cavity-mediated interactions reshape material properties in the multimode ultrastrong coupling regime [65]. In Landau polariton systems, this question of cavity mediation is particularly compelling because the cavity can couple both to the local $k = 0$ cyclotron resonance and to nonlocal finite-k magnetoplasmons.

No detectable pairwise entanglement emerges between any pair of matter modes across the investigated magnetic field range, even though the cavity redistributes vacuum entanglement predominantly into the a_- sector (as detailed in Supplementary Note 5). Nevertheless, Fig. 3b shows that all matter pairs exhibit finite Gaussian discord throughout the magnetic field range. Correlations involving the cyclotron resonance are the strongest, while the MP_1–MP_3 pair remains weaker but nonclassically correlated. The cavity therefore imprints a quantum correlation structure inside the matter subsystem, but in a nontrivial form beyond pairwise entanglement: the matter modes remain separable, yet they are nonclassically correlated. Together with the finite a_-–matter correlations in Fig. 3a, this correlation hierarchy points to a collective a_--centered correlated sector rather than to independent matter–matter pairs.

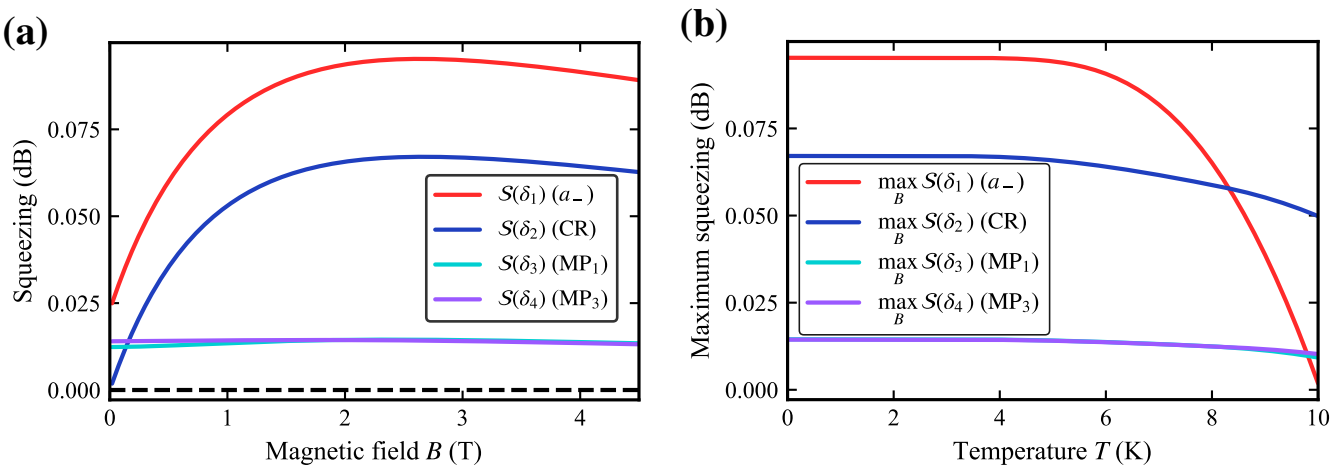


FIG. 4: Nullifier squeezing and thermal robustness of the vacuum graph state. **(a)** Nullifier squeezing, Eq. 39 of Supplementary Note 7, of the reduced four mode sector $\{a_-, \mathrm{CR}, \mathrm{MP}_1, \mathrm{MP}_3\}$, showing simultaneous subvacuum suppression of the optimized graph state nullifiers. **(b)** Thermal robustness of the vacuum correlation structure. The maximum nullifier squeezing remains essentially unchanged in the cryogenic regime and decreases only when thermal populations become appreciable.

A nearly isolated a_--centered sector hosting graph-like vacuum correlations. The hierarchy established above suggests that the relevant correlated object is the reduced sector $\{a_-, \mathrm{CR}, \mathrm{MP}_1, \mathrm{MP}_3\}$. This sector behaves as a nearly isolated correlated subsystem, as indicated by the high purity of the reduced state $\rho_{a_-,\mathrm{CR},\mathrm{MP}_1,\mathrm{MP}_3}$. As shown in Fig. 6c of Supplementary Note 5, the purity remains extremely close to unity throughout the full magnetic field range, with $\mu > 0.999$ for the present parameter set. The spectroscopically active polarization a_+ is only weakly connected to the dominant correlated sector, so tracing it out introduces very little mixedness. This point is important conceptually as inseparability across all bipartitions certifies genuine multipartite entanglement in the pure state limit [66]. Here the reduced state is not strictly pure, but its near unity purity allows the multipartite structure evidenced by the bipartition analysis in Supplementary Note 7 to be effectively interpreted as a genuinely multipartite entangled sector.

Having established the near isolation and multipartite character of this sector, we next ask whether its correlations possess an organized graph-like form. We therefore examine the continuous variable nullifiers, Eq. 39 of Supplementary Note 7, constructed from the effective adjacency matrix of the reduced covariance matrix [36, 47, 48]. The construction of the effective adjacency matrix and the optimized nullifier variances is detailed in Supplementary Note 7. Figure 4a shows that all optimized nullifiers exhibit positive squeezing in dB throughout the magnetic field range. Equivalently, their variances remain below the vacuum limit of $1/2$, demonstrating simultaneous subvacuum suppression in the linear combinations that define the effective graph structure. The strongest squeezing is associated with a_- and the cyclotron mode, while the magnetoplasmon nullifiers exhibit weaker but still systematic suppression, reproducing the hierarchy already visible in the correlation measures.

These results support the graph-like interpretation anticipated schematically in Fig. 1c. Because the reduced state is nearly pure and its nullifiers are simultaneously squeezed, the covariance matrix is consistent with an effective Gaussian graph state description in which a_- acts as the central hub, while the matter excitations form the surrounding nodes. The extracted adjacency matrix shown in Fig. 8c of Supplementary Note 7 reflects the same structure, with the strongest edge associated with the a_-–CR connection. In this sense, the structured vacuum correlations are neither random nor merely spectroscopic by-products of hybridization; they organize into a coherent multipartite sector selected by the inactive polarization.

Taken together, the purity, bipartition structure, and nullifier squeezing identify $\{a_-, \mathrm{CR}, \mathrm{MP}_1, \mathrm{MP}_3\}$ as a nearly isolated a_--centered sector with effective multipartite entanglement and an internal graph-like organization.

Thermal robustness in the cryogenic regime. The four mode vacuum correlation structure remains robust throughout the cryogenic temperature window typically explored in Landau polariton experiments [17, 20, 21]. As shown in Fig. 4b, the maximum nullifier squeezing is essentially unchanged up to about 4–5 K, including the 1.6 K experimental condition of the device considered here [24]. At higher temperatures, thermal populations progressively wash out the anomalous correlations that underlie the graph-like vacuum structure, and the nullifier squeezing decreases accordingly.

This reduction is not uniform across the four nodes: the squeezing associated with a_- drops faster than the others. Such behavior is consistent with the finite temperature form of the anomalous correlators, in which Bose Einstein occupations dress the pairing channels responsible for the ground state squeezing. Because the dominant anomalous structure of the

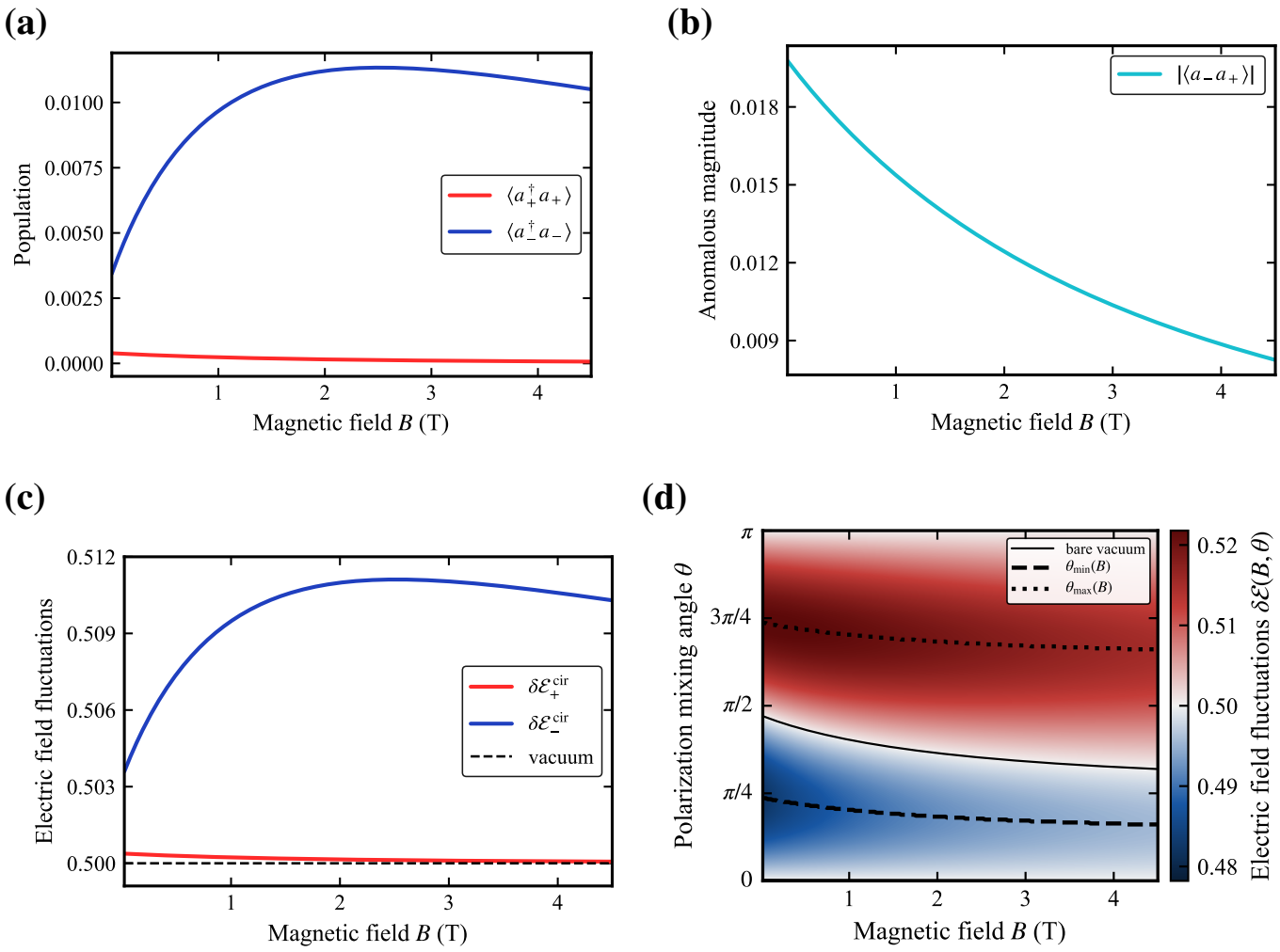


FIG. 5: Polarization anisotropy of dressed vacuum field fluctuations. **(a)** Photonic populations in the dressed ground state, showing the unequal dressing of the two circular cavity modes. **(b)** Magnitude of the anomalous correlation between the circular modes, which contributes to the mixing angle dependence of field fluctuations. **(c)** Circular basis electric field fluctuations, Eq. (15), relative to the bare vacuum level. The active circular component remains close to the vacuum value, whereas the orthogonal component develops enhanced dressed vacuum fluctuations. **(d)** Electric field fluctuation $\delta\mathcal{E}(B,\theta)$, Eq. (17), map as a function of magnetic field and polarization mixing angle. The black solid line marks the bare vacuum level, while the dashed and dotted curves indicate the polarization mixing angles of minimum and maximum fluctuation. The resulting anisotropy provides a field level signature of the chiral routing of vacuum correlations into the a_--dominated sector.

correlated sector is routed through a_-, its nullifier is affected by thermal admixture through the largest set of relevant channels. The centrality that makes a_- the strongest squeezed node in the ground state therefore also makes it the most thermally fragile component of the four mode structure.

Polarization resolved vacuum field fluctuations revealing the chiral vacuum structure. Having established that chiral symmetry routes the dominant anomalous correlations into the inactive polarization sector, we now ask how the same symmetry shapes the cavity vacuum electric field. We define the Hermitian electric field quadratures associated with the two circular cavity modes, following [29], as

$$E_\pm^{\rm cir} = iE_0\big(a_\pm^\dagger - a_\pm\big), \tag{13}$$

where E_0 denotes the single-mode vacuum electric-field amplitude at the evaluation point, determined by the cavity mode profile. Then, the dressed vacuum fluctuations of each circular component can be characterized by

$$\delta\mathcal{E}_\pm^{\rm cir}(B) = \frac{\langle(\Delta E_\pm^{\rm cir})^2\rangle}{2E_0^2}, \tag{14}$$

which reduces to the shot-noise limit of $1/2$ in the uncoupled bare vacuum limit.

The circular basis already exposes the chiral hierarchy. Because self-anomalous correlators are forbidden by the chiral selection rule, the variance of each circular field reduces to

$$\delta\mathcal{E}_{\pm}^{\mathrm{cir}} = \frac{1}{2} + \langle a_{\pm}^{\dagger} a_{\pm} \rangle, \tag{15}$$

so that $\delta\mathcal{E}_{\pm}^{\mathrm{cir}}$ directly tracks the corresponding virtual photon population $n_{\pm} = \langle a_{\pm}^{\dagger} a_{\pm} \rangle$. The active circular component then remains essentially at the bare vacuum level because n_{+} is negligible, whereas the orthogonal polarization develops enhanced fluctuations with increasing magnetic field due to the growth of n_{-}, as shown in panel (a) and (c) of Fig. 5. In this way, circular electric fields reflect the asymmetric dressing of the two circular cavity components enforced by chirality.

A general polarization-resolved field measurement, however, does not need to align with either circular component. We therefore define a Hermitian quadrature parameterized by a polarization mixing angle θ

$$E_{\theta} = \cos\theta\, E_{+}^{\mathrm{cir}} + \sin\theta\, E_{-}^{\mathrm{cir}}, \tag{16}$$

and its normalized vacuum fluctuations

$$\delta\mathcal{E}(B,\theta) = \frac{\langle (\Delta E_{\theta})^2 \rangle}{2E_0^2}. \tag{17}$$

In terms of the underlying mode operators, this variance contains the two circular population contributions and an interference term,

$$\delta\mathcal{E}(B,\theta) = \frac{1}{2} + \cos^2\theta\, n_{+} + \sin^2\theta\, n_{-} - \sin(2\theta)\,\mathrm{Re}\,\langle a_{+} a_{-} \rangle. \tag{18}$$

The first three terms describe the enhancement of field fluctuations above the bare vacuum level of $1/2$, arising from the presence of virtual populations $n_{\pm}$. In this way, vacuum fluctuations provide an indirect probe of virtual particles through measurable noisy field signatures. The last term, proportional to the anomalous correlator $\langle a_{+} a_{-} \rangle$, represents an interference contribution that can suppress the fluctuations and even squeeze them below the shot-noise limit. This interference between the two circular components fades with increasing magnetic field (panel (b) of Fig. 5). Both effects depend strongly on the magnetic field B, which controls the virtual populations and the strength of the anomalous correlations, and on the polarization mixing angle θ, which reflects the anisotropic nature of the dressed vacuum. If the cavity vacuum were trivial, *i.e.*, in the absence of virtual populations and anomalous correlations, the field fluctuations would remain at the bare vacuum level, yielding $\delta\mathcal{E}(B,\theta) = 1/2$ for all polarization mixing. Therefore, the robust angular dependence of Eq. (17) shown in Figure 5d, is not an independent effect on top of the correlation analysis, but the field level manifestation of the same chiral routing mechanism.

DISCUSSION

We showed that chiral ultrastrong coupling separates two roles of the cavity that are often implicitly associated with one another. In the Landau polariton system studied here, the polarization a_{+} remains the spectroscopically bright channel that organizes the avoided crossings, while the dominant anomalous correlators, vacuum squeezing, and cavity–matter entanglement are routed into the orthogonal polarization a_{-}. The polarization that forms the observed polariton branches is not necessarily the one that carries the nonclassical structure of the ground state [24, 29, 51]. This distinction is essential for controlling cavity of matter as recent theory has emphasized that light–matter entanglement can be an essential ingredient through which cavity quantum materials can modify some properties via vacuum field engineering [61, 67–69]. In Landau polariton systems, cavity vacuum fields are already known to influence equilibrium transport and collective properties of a two-dimensional electron gas [16–18, 50]. The implication of our results is that spectroscopy and quantum information diagnostics answer complementary questions: the former determines mode hybridization, while the latter reveals which light and matter degrees of freedom share nonclassical correlations in the dressed vacuum.

The polarization-resolved field fluctuation anisotropy gives this hidden structure a signature at the field level. In the circular basis, the field fluctuation of each component directly tracks the corresponding virtual population because same-polarization anomalous moments are forbidden by the chiral symmetry. In a general mixed polarization, the anomalous correlation between the two circular components enters as an interference term, enhancing or suppressing the dressed vacuum noise depending on the mixing angle. The vacuum noise therefore acquires an angular texture set by the chiral routing of correlations. This connects naturally to electro-optic measurements of electromagnetic vacuum field correlations in the terahertz range, which have shown that vacuum field correlations can be accessed without relying on photon emission or intensity detection [19]. In this sense, the predicted anisotropy serves as an experimentally accessible fingerprint of the hidden non-polaritonic vacuum sector.

The hidden correlated sector has a well defined internal organization. The mode a_- acts as the hub of the vacuum structure: it carries the strongest cavity–matter entanglement, mediates finite Gaussian discord between cyclotron and magnetoplasmon excitations, and forms, together with $\{\mathrm{CR}, \mathrm{MP}_1, \mathrm{MP}_3\}$, a nearly pure state consistent with an effective Gaussian graph state description [36, 48, 70, 71]. By contrast, a_+ is only weakly and indirectly connected to this structure. The cavity therefore does more than produce avoided crossings: it redistributes nonclassical correlations across distinct collective channels of the 2DEG. In particular, the finite matter–matter quantum discord shows that local cyclotron and nonlocal magnetoplasmon modes can remain quantum correlated even when they are not pairwise entangled. This identifies Gaussian discord as an indicator of the hidden vacuum structure of the cavity.

More broadly, our findings point to a passive route toward structured correlated vacua in solid state cavity QED. In contrast to optical continuous variable graph states generated by external driving or nonlinear state preparation [72, 73], the graph-like multimode Gaussian structure identified here emerges directly from symmetry and counter-rotating interactions in equilibrium. It complements recent studies of ground state entanglement and nonclassical ultrastrong-coupling vacua in bosonic and polaritonic settings [70, 71], but adds an organizing principle based on symmetry: chirality determines not only which excitations are bright, but also how the vacuum correlations are routed.

This perspective suggests several directions. First, polarization-resolved field correlation or response measurements could provide direct tests of the predicted asymmetry between the bright spectroscopic channel and the hidden vacuum correlation channel. Second, the matter sector discord found here motivates further study of whether non-entangling quantum correlations can influence equilibrium electronic response, especially in settings where cavity vacuum fields already modify transport. Third, the same routing principle may be engineered beyond Landau polaritons. In superconducting circuits, ingredients related to chirality and synthetic angular-momentum structure have already been demonstrated in few qubit architectures [74]. Atomic platforms likewise offer a high degree of control over motional and spin–motion degrees of freedom [75, 76], and chiral quantum-optical couplings have been proposed more explicitly in Rydberg and trapped-ion settings [77].

In conlusion, our results recast chirality as more than a selection rule for polariton spectroscopy. It is a symmetry principle for organizing the ultrastrong coupling vacuum itself. The chiral structure of Landau polaritons separates the bright polariton spectrum from the hidden nonclassical vacuum sector while imprinting a polarization anisotropy in the field fluctuations, thereby opening a route to explore how cavity-mediated quantum correlations, including correlations beyond entanglement, may enter the equilibrium physics of quantum materials.

METHODS

Chiral charge and closed operator sectors. The schematic Hamiltonian in Eq. (1) has a conserved chiral charge

$$Q = a_+^\dagger a_+ + \sum_j m_j^\dagger m_j - a_-^\dagger a_-, \tag{19}$$

which assigns charge -1 to a_+ and the matter annihilation operators m_j, and charge $+1$ to a_-. The corresponding $U(1)$ unitary transformation $U(\theta) = e^{-i\theta Q}$ gives

$$U^\dagger(\theta) a_+ U(\theta) = e^{-i\theta} a_+, \tag{20}$$

$$U^\dagger(\theta) m_j U(\theta) = e^{-i\theta} m_j, \tag{21}$$

$$U^\dagger(\theta) a_- U(\theta) = e^{+i\theta} a_-. \tag{22}$$

Every term in Eq. (1) is neutral under this transformation, and therefore

$$[H, Q] = 0. \tag{23}$$

The same symmetry appears dynamically as a block decomposition of the Heisenberg equations. Direct evaluation gives

$$i\dot{a}_+ = (\omega_0 + D)\, a_+ + D\, a_-^\dagger - i \sum_j g_j m_j, \tag{24}$$

$$i\dot{m}_j = \omega_j m_j + i g_j (a_+ + a_-^\dagger), \tag{25}$$

$$i\dot{a}_-^\dagger = -(\omega_0 + D) a_-^\dagger - D a_+ + i \sum_j g_j m_j. \tag{26}$$

Thus the negative-charge operator vector

$$\boldsymbol{\eta}_- = (a_+, m_1, m_2, \ldots, a_-^\dagger)^T \tag{27}$$

is closed under time evolution, $i\dot{\eta}_- = K_-\boldsymbol{\eta}_-$, with

$$K_- = \begin{pmatrix} \omega_0 + D & -ig_1 & -ig_2 & \cdots & -ig_{N_m} & D \\ ig_1 & \omega_1 & 0 & \cdots & 0 & ig_1 \\ ig_2 & 0 & \omega_2 & \cdots & 0 & ig_2 \\ \vdots & \vdots & \vdots & \ddots & \vdots & \vdots \\ ig_{N_m} & 0 & 0 & \cdots & \omega_{N_m} & ig_{N_m} \\ -D & ig_1 & ig_2 & \cdots & ig_{N_m} & -(\omega_0 + D) \end{pmatrix}. \tag{28}$$

The Hermitian conjugate positive charge sector

$$\boldsymbol{\eta}_+ = (a_+^\dagger, m_1^\dagger, m_2^\dagger, \ldots, a_-)^T \tag{29}$$

is also closed, so that

$$i\frac{d}{dt}\begin{pmatrix}\boldsymbol{\eta}_- \\ \boldsymbol{\eta}_+\end{pmatrix} = \begin{pmatrix} K_- & 0 \\ 0 & K_+ \end{pmatrix}\begin{pmatrix}\boldsymbol{\eta}_- \\ \boldsymbol{\eta}_+\end{pmatrix}, \qquad K_+ = -K_-^*. \tag{30}$$

Selection rule for anomalous moments. The block structure above is equivalent to a charge selection rule. Let O_q be an operator with definite chiral charge q, such that

$$U^\dagger(\theta) O_q U(\theta) = e^{-iq\theta} O_q. \tag{31}$$

Since $[H, Q] = 0$, a nondegenerate ground state can be chosen as an eigenstate of Q. Therefore,

$$\begin{aligned} \langle O_q \rangle &= \langle \mathrm{GS}| \, O_q \, |\mathrm{GS}\rangle \\ &= \langle \mathrm{GS}| \, U^\dagger(\theta) O_q U(\theta) \, |\mathrm{GS}\rangle \\ &= e^{-iq\theta}\langle O_q \rangle, \end{aligned} \tag{32}$$

for arbitrary θ. Hence $\langle O_q \rangle = 0$ unless $q = 0$.

Applying this rule to the anomalous correlators involving the spectroscopically active polarization gives

$$q(a_+ a_+) = -2, \qquad q(a_+ m_j) = -2, \qquad q(a_+^\dagger m_j^\dagger) = +2, \tag{33}$$

and therefore

$$\langle a_+ a_+ \rangle = 0, \qquad \langle a_+ m_j \rangle = 0, \qquad \langle a_+^\dagger m_j^\dagger \rangle = 0. \tag{34}$$

Thus all anomalous correlators involving a_+ and matter annihilation operators vanish identically in any Q-eigenstate, including the ground state. By contrast, anomalous correlators involving the inactive polarization a_-, such as $\langle a_- m_j \rangle$ in the charge balanced sector or equivalently the corresponding quadrature correlations generated by counter rotating terms, are not forbidden by the $U(1)$ symmetry. This is the origin of the selection rule of the vacuum correlation routing discussed in the main text.

Perturbations that mix circular polarizations, such as cavity birefringence, ellipticity, or breaking of the ideal selection rules by disorder, do not commute with Q. Such terms can activate otherwise forbidden anomalous correlators involving a_+ and provide a direct way to test the robustness of the chiral hierarchy.

Bogoliubov diagonalization and covariance matrix construction. The chiral block decomposition allows the Bogoliubov problem to be formulated separately in the two charge sectors. In the negative charge sector,

$$\boldsymbol{\eta}_- = (a_+, m_1, m_2, \ldots, a_-^\dagger)^T, \tag{35}$$

we define normal mode operators

$$P_{\nu,-} = w_{\nu,+}\, a_+ + \sum_j w_{\nu,j}\, m_j + y_{\nu,-}\, a_-^\dagger, \tag{36}$$

which satisfy

$$[P_{\nu,-}, H] = \Omega_{\nu,-} P_{\nu,-}. \tag{37}$$

This sector contains the active cavity annihilation operator a_+ and the matter annihilation operators m_j, and therefore hosts the polariton branches observed in the active spectroscopic response. The inactive polarization enters this sector only through $a_-^\dagger$, i.e. through the counter-rotating component.

The positive charge sector,

$$\boldsymbol{\eta}_+ = (a_+^\dagger, m_1^\dagger, m_2^\dagger, \ldots, a_-)^T, \tag{38}$$

is diagonalized analogously by

$$P_{\nu,+} = \tilde{y}_{\nu,+}\, a_+^\dagger + \sum_j \tilde{y}_{\nu,j}\, m_j^\dagger + \tilde{w}_{\nu,-}\, a_-, \tag{39}$$

with

$$[P_{\nu,+}, H] = \Omega_{\nu,+} P_{\nu,+}. \tag{40}$$

For the ideal chiral Hamiltonian considered here, the two blocks are related by Hermitian conjugation, $K_+ = -K_-^*$. Consequently, the positive frequency spectrum of the full Bogoliubov problem can be obtained from either block together with its conjugate partner. In practice, we retain all positive norm, positive frequency solutions and normalize them with the bosonic metric,

$$|w_{\nu,+}|^2 + \sum_j |w_{\nu,j}|^2 - |y_{\nu,-}|^2 = 1 \tag{41}$$

for the $\boldsymbol{\eta}_-$ sector, and similarly for $\boldsymbol{\eta}_+$. The quadratic Hamiltonian then takes the diagonal form

$$H = \sum_{\nu,s=\pm} \Omega_{\nu,s}\, P_{\nu,s}^\dagger P_{\nu,s}, \tag{42}$$

up to the ground state energy, where only positive frequency normal modes are included.

The covariance matrix is obtained from Gaussian contractions in the normal mode basis. Since the Hamiltonian is quadratic, the ground state and the finite temperature Gibbs state are Gaussian. Therefore, all second moments of the bare operators follow from Wick contractions once the normal mode occupations are specified. At zero temperature,

$$\langle P_{\nu,s}^\dagger P_{\mu,s'} \rangle = 0, \qquad \langle P_{\nu,s} P_{\mu,s'}^\dagger \rangle = \delta_{\nu\mu}\delta_{ss'}. \tag{43}$$

At finite temperature,

$$\begin{aligned} \langle P_{\nu,s}^\dagger P_{\mu,s'} \rangle &= n_{\nu,s}(T)\, \delta_{\nu\mu}\delta_{ss'}, \\ \langle P_{\nu,s} P_{\mu,s'}^\dagger \rangle &= \big[n_{\nu,s}(T) + 1\big]\delta_{\nu\mu}\delta_{ss'}. \end{aligned} \tag{44}$$

where

$$n_{\nu,s}(T) = \frac{1}{\exp(\beta\Omega_{\nu,s}) - 1}. \tag{45}$$

Substituting the inverse Bogoliubov transformation then gives the normal and anomalous correlators among the physical cavity and matter modes. These include, for example, $\langle a_\xi^\dagger a_{\xi'} \rangle$, $\langle m_i^\dagger m_j \rangle$, $\langle a_\xi m_j \rangle$, and $\langle a_\xi a_{\xi'} \rangle$, which are the ingredients entering the quadrature covariance matrix.

We introduce dimensionless quadratures for each physical mode,

$$x_\ell = \frac{o_\ell + o_\ell^\dagger}{\sqrt{2}}, \qquad p_\ell = \frac{o_\ell - o_\ell^\dagger}{i\sqrt{2}}, \tag{46}$$

where

$$\{o_\ell\} = \{a_+, a_-, m_1, m_2, \ldots\}. \tag{47}$$

Collecting them into

$$\boldsymbol{R} = (x_1, p_1, x_2, p_2, \ldots, x_N, p_N)^T, \tag{48}$$

the covariance matrix is

$$V_{jk} = \frac{1}{2}\langle R_j R_k + R_k R_j \rangle. \tag{49}$$

The symplectic form is

$$\Omega = \bigoplus_{\ell=1}^{N} \begin{pmatrix} 0 & 1 \\ -1 & 0 \end{pmatrix}, \tag{50}$$

so that $[R_j, R_k] = i\Omega_{jk}$. In this convention the bare vacuum satisfies $V_{\mathrm{vac}} = I/2$, and any physical covariance matrix obeys

$$V + \frac{i}{2}\Omega \geq 0. \tag{51}$$

Numerical checks of the Bogoliubov transformation and covariance matrix physicality are reported in Supplementary Note 2.

All purity, entanglement, discord, and graph state diagnostics used in the main text are obtained directly from the covariance matrix V, Eq. (51). In practice, this reduces the analysis to standard linear algebra operations. Selecting subsets of quadratures to construct reduced covariance matrices, computing symplectic eigenvalues for entropies and mutual information, applying partial transposition to evaluate logarithmic negativities, optimizing the Gaussian conditional entropy for the Gaussian discord, and extracting the effective adjacency matrix that minimizes the nullifier variances.

DATA AVAILABILITY

The datasets used and/or analyzed during the current study are available from the following publicly accessible repository https://github.com/MoorishQubit/Hopfield.

CODE AVAILABILITY

The source code to reproduce the results and all the data used to generate the plots is available in the accompanying GitHub repository https://github.com/MoorishQubit/Hopfield.

ACKNOWLEDGEMENTS

Z.M. acknowledges funding from the Ministry of Economic Affairs, Labour and Tourism Baden-Württemberg in the frame of the Competence Center Quantum Computing Baden-Württemberg (project "KQCBW25"). H.R.'s material is based upon work supported by the Department of Energy [Basic Energy Sciences] under Award Number(s) [DE-FG02-02ER15344].

AUTHOR CONTRIBUTIONS

A.E.-A. and Z.M. conceived the research project, developed the theoretical framework, derived the analytical results, and performed the numerical simulations. H.S. contributed to the theoretical analysis, interpretation of the results, and scientific discussions. H.R., A.E.F. and D.L. supervised the research and provided critical feedback throughout the project. All authors contributed to the writing and revision of the manuscript and approved the final version.

COMPETING INTERESTS

The authors declare no competing interests.

---

* ayoub.el-amrani@um6p.ma
† dukhyung.lee@um6p.ma

[1] P. Forn-Díaz, L. Lamata, E. Rico, J. Kono, and E. Solano, Ultrastrong coupling regimes of light-matter interaction, Rev. Mod. Phys. **91**, 025005 (2019).
[2] A. F. Kockum, A. Miranowicz, S. De Liberato, S. Savasta, and F. Nori, Ultrastrong coupling between light and matter, Nat. Rev. Phys. **1**, 19 (2019).
[3] C. Schäfer, M. Ruggenthaler, V. Rokaj, and A. Rubio, Relevance of the quadratic diamagnetic and self-polarization terms in cavity quantum electrodynamics, ACS Photonics **7**, 975 (2020).
[4] J. J. Hopfield, Theory of the contribution of excitons to the complex dielectric constant of crystals, Phys. Rev. **112**, 1555 (1958).
[5] C. Ciuti, G. Bastard, and I. Carusotto, Quantum vacuum properties of the intersubband cavity polariton field, Phys. Rev. B **72**, 115303 (2005).
[6] S. De Liberato, Virtual photons in the ground state of a dissipative system, Nat. Commun. **8**, 1465 (2017).
[7] S. Ashhab and F. Nori, Qubit-oscillator systems in the ultrastrong-coupling regime and their potential for preparing nonclassical states, Phys. Rev. A **81**, 042311 (2010).
[8] C. Hotter, A. Miranowicz, and K. Gietka, Quantum metrology in the ultrastrong coupling regime of light-matter interactions: Leveraging virtual excitations without extracting them, Phys. Rev. Lett. **135**, 100802 (2025).
[9] A. Baydin, H. Zhu, M. Bamba, K. Hazzard, and J. Kono, Perspective on the quantum vacuum in matter, Opt. Mater. Express **15**, 1833 (2025).
[10] S. De Liberato, C. Ciuti, and I. Carusotto, Quantum vacuum radiation spectra from a semiconductor microcavity with a time-modulated vacuum rabi frequency, Phys. Rev. Lett. **98**, 103602 (2007).
[11] R. Stassi, A. Ridolfo, O. Di Stefano, M. J. Hartmann, and S. Savasta, Spontaneous conversion from virtual to real photons in the ultrastrong-coupling regime, Phys. Rev. Lett. **110**, 243601 (2013).
[12] M. Cirio, S. D. Liberato, N. Lambert, and F. Nori, Ground state electroluminescence, Physical Review Letters **116**, 113601 (2016).

[13] M. Cirio, N. Shammah, N. Lambert, S. De Liberato, and F. Nori, Multielectron ground state electroluminescence, Phys. Rev. Lett. **122**, 190403 (2019).

[14] G. Falci, A. Ridolfo, P. G. Di Stefano, *et al.*, Ultrastrong coupling probed by coherent population transfer, Sci. Rep. **9**, 9249 (2019).

[15] A. Ridolfo, J. Rajendran, L. Giannelli, *et al.*, Probing ultrastrong light–matter coupling in open quantum systems, Eur. Phys. J. Spec. Top. **230**, 941 (2021).

[16] N. Bartolo and C. Ciuti, Vacuum-dressed cavity magnetotransport of a two-dimensional electron gas, Phys. Rev. B **98**, 205301 (2018).

[17] G. L. Paravicini-Bagliani, F. Appugliese, E. Richter, F. Valmorra, J. Keller, M. Beck, N. Bartolo, C. Rössler, T. Ihn, K. Ensslin, C. Ciuti, G. Scalari, and J. Faist, Magneto-transport controlled by landau polariton states, Nature Physics **15**, 186 (2019).

[18] F. Appugliese, J. Enkner, G. L. Paravicini-Bagliani, M. Beck, C. Reichl, W. Wegscheider, G. Scalari, C. Ciuti, and J. Faist, Breakdown of topological protection by cavity vacuum fields in the integer quantum hall effect, Science **375**, 1030 (2022).

[19] I.-C. Benea-Chelmus, F. F. Settembrini, G. Scalari, and J. Faist, Electric field correlation measurements on the electromagnetic vacuum state, Nature **568**, 202 (2019).

[20] G. Scalari, C. Maissen, D. Turčinková, D. Hagenmüller, S. De Liberato, C. Ciuti, C. Reichl, D. Schuh, W. Wegscheider, M. Beck, and J. Faist, Ultrastrong coupling of the cyclotron transition of a 2d electron gas to a thz metamaterial, Science **335**, 1323 (2012).

[21] Q. Zhang, M. Lou, X. Li, J. L. Reno, W. Pan, J. D. Watson, M. J. Manfra, and J. Kono, Collective non-perturbative coupling of 2d electrons with high-quality-factor terahertz cavity photons, Nat. Phys. **12**, 1005 (2016).

[22] J. Keller, G. Scalari, S. Cibella, X. Li, R. Zhao, G. Paravicini-Bagliani, J. Kono, and J. Faist, Landau polaritons in highly non-parabolic two-dimensional gases in the ultrastrong coupling regime, Phys. Rev. B **101**, 075301 (2020).

[23] J. Mornhinweg, L. K. Diebel, M. Halbhuber, M. Prager, J. Riepl, T. Inzenhofer, D. Bougeard, R. Huber, C. Lange, *et al.*, Mode-multiplexing deep-strong light-matter coupling, Nat. Commun. **15**, 1847 (2024).

[24] S. R. Endo, D. Kim, S. Liang, G. Lee, S. Kim, A. Covarrubias-Morales, M. Seo, M. J. Manfra, D. Lee, M. Bamba, and J. Kono, Cavity-mediated coupling between local and nonlocal modes in landau polaritons, Nanophotonics **14**, 4647 (2025).

[25] Z. A. VanOrman, W. R. Kitzmann, A. P. M. Reponen, *et al.*, Chiral light–matter interactions in solution-processable semiconductors, Nature Reviews Chemistry **9**, 208 (2025).

[26] F. Tay, S. Sanders, A. Baydin, *et al.*, Terahertz chiral photonic-crystal cavities for dirac gap engineering in graphene, Nature Communications **16**, 5270 (2025).

[27] J. Andberger, L. Graziotto, L. Sacchi, M. Beck, G. Scalari, and J. Faist, Terahertz chiral subwavelength cavities breaking time-reversal symmetry via ultrastrong light-matter interaction, Phys. Rev. B **109**, L161302 (2024).

[28] L. Yang, G. Cardoso, T. H. Hansson, and Q.-D. Jiang, Quantum hall effect in a chiral cavity, Phys. Rev. B **113**, 045109 (2026).

[29] X. Li, M. Bamba, Q. Zhang, *et al.*, Vacuum bloch–siegert shift in landau polaritons with ultra-high cooperativity, Nature Photonics **12**, 324 (2018).

[30] C. Weedbrook, S. Pirandola, R. García-Patrón, N. J. Cerf, T. C. Ralph, J. H. Shapiro, and S. Lloyd, Gaussian quantum information, Rev. Mod. Phys. **84**, 621 (2012).

[31] A. Ferraro, S. Olivares, and M. G. A. Paris, Gaussian states in continuous variable quantum information (2005), arXiv:quant-ph/0503237 [quant-ph].

[32] S. L. Braunstein and P. van Loock, Quantum information with continuous variables, Rev. Mod. Phys. **77**, 513 (2005).

[33] J. Eisert and M. B. Plenio, Introduction to the basics of entanglement theory in continuous-variable systems, Int. J. Quant. Inf. **1**, 479 (2003).

[34] S. L. Braunstein and H. J. Kimble, Teleportation of continuous quantum variables, Phys. Rev. Lett. **80**, 869 (1998).

[35] S. Lloyd and S. L. Braunstein, Quantum computation over continuous variables, Phys. Rev. Lett. **82**, 1784 (1999).

[36] N. C. Menicucci, P. van Loock, M. Gu, C. Weedbrook, T. C. Ralph, and M. A. Nielsen, Universal quantum computation with continuous-variable cluster states, Phys. Rev. Lett. **97**, 110501 (2006).

[37] J. I. Latorre and A. Riera, A short review on entanglement in quantum spin systems, Journal of Physics A: Mathematical and Theoretical **42**, 504002 (2009).

[38] A. Osterloh, L. Amico, G. Falci, and R. Fazio, Scaling of entanglement close to a quantum phase transition, Nature **416**, 608 (2002).

[39] T. J. Osborne and M. A. Nielsen, Entanglement in a simple quantum phase transition, Physical Review A **66**, 032110 (2002).

[40] G. Vidal, J. I. Latorre, E. Rico, and A. Kitaev, Entanglement in quantum critical phenomena, Physical Review Letters **90**, 227902 (2003).

[41] L. Amico, R. Fazio, A. Osterloh, and V. Vedral, Entanglement in many-body systems, Reviews of Modern Physics **80**, 517 (2008).

[42] Z. Mzaouali and M. E. Baz, Long range quantum coherence, quantum & classical correlations in heisenberg xx chain, Physica A: Statistical Mechanics and its Applications **518**, 119 (2019).

[43] Z. Mzaouali, S. Campbell, and M. E. Baz, Discrete and generalized phase space techniques in critical quantum spin chains, Physics Letters A **383**, 125932 (2019).

[44] K. E. Hawary, M. Azzouz, M. E. Baz, S. Deffner, B. Gardas, and Z. Mzaouali, Navigating the phase diagram of quantum many-body systems in phase space, Physical Review E **110**, 014120 (2024).

[45] S. Abaach, Z. Mzaouali, and M. E. Baz, Long distance entanglement and high-dimensional quantum teleportation in the fermi–hubbard model, Scientific Reports **13**, 964 (2023).

[46] Z. Mzaouali, R. Puebla, J. Goold, M. El Baz, and S. Campbell, Work statistics and symmetry breaking in an excited-state quantum phase transition, Phys. Rev. E **103**, 032145 (2021).
[47] J. Zhang and S. L. Braunstein, Continuous-variable gaussian analog of cluster states, Phys. Rev. A **73**, 032318 (2006).
[48] N. C. Menicucci, S. T. Flammia, and P. van Loock, Graphical calculus for gaussian pure states, Phys. Rev. A **83**, 042335 (2011).
[49] F. Mivehvar, Driven-dissipative landau polaritons: Two highly nonlinearly coupled quantum harmonic oscillators, Physical Review Letters **136**, 093602 (2026), arXiv:2509.12321 [cond-mat.str-el].
[50] J. Enkner, L. Graziotto, D. Boriçi, and et al., Tunable vacuum-field control of fractional and integer quantum hall phases, Nature **641**, 884 (2025).
[51] S. Mahmoodian, Chiral light-matter interaction beyond the rotating-wave approximation, Phys. Rev. Lett. **123**, 133603 (2019).
[52] S. Scheel and D.-G. Welsch, Entanglement generation and degradation by passive optical devices, Phys. Rev. A **64**, 063811 (2001).
[53] M. S. Kim, W. Son, V. Bužek, and P. L. Knight, Entanglement by a beam splitter: Nonclassicality as a prerequisite for entanglement, Phys. Rev. A **65**, 032323 (2002).
[54] W. Xiang-bin, Theorem for the beam-splitter entangler, Phys. Rev. A **66**, 024303 (2002).
[55] C. Maissen, G. Scalari, F. Valmorra, M. Beck, J. Faist, S. Cibella, R. Leoni, C. Reichl, C. Charpentier, and W. Wegscheider, Ultrastrong coupling in the near field of complementary split-ring resonators, Phys. Rev. B **90**, 205309 (2014).
[56] S. Rajabali, S. Markmann, E. Jöchl, M. Beck, H. Li, V. Mailaender, M. Volkmann, U. Schade, G. Scalari, M. Rajabali, and J. Faist, An ultrastrongly coupled single terahertz meta-atom, Nature Communications **13**, 2528 (2022).
[57] H. Ollivier and W. H. Zurek, Quantum discord: A measure of the quantumness of correlations, Phys. Rev. Lett. **88**, 017901 (2001).
[58] L. Henderson and V. Vedral, Classical, quantum and total correlations, Journal of Physics A: Mathematical and General **34**, 6899 (2001).
[59] G. Adesso and A. Datta, Quantum versus classical correlations in gaussian states, Phys. Rev. Lett. **105**, 030501 (2010).
[60] P. Giorda and M. G. A. Paris, Gaussian quantum discord, Phys. Rev. Lett. **105**, 020503 (2010).
[61] F. J. Garcia-Vidal, C. Ciuti, and T. W. Ebbesen, Manipulating matter by strong coupling to vacuum fields, Science **373**, eabd0336 (2021).
[62] C. Schäfer, J. Flick, E. Ronca, P. Narang, and A. Rubio, Shining light on the microscopic resonant mechanism responsible for cavity-mediated chemical reactivity, Nature Communications **13**, 7817 (2022).
[63] D. Kim, J. Hou, G. Lee, *et al.*, Multimode phonon-polaritons in lead-halide perovskites in the ultrastrong coupling regime, Nat. Commun. **16**, 8658 (2025).
[64] F. Tay, A. Mojibpour, S. Sanders, *et al.*, Multimode ultrastrong coupling in three-dimensional photonic-crystal cavities, Nat. Commun. **16**, 3603 (2025).
[65] H. Liu, F. Troisi, H. Hübener, S. Latini, and A. Rubio, Cavity-mediated electron-electron interactions: Renormalizing dirac states in graphene, Science Advances **11**, eadz1855 (2025).
[66] O. Gühne and G. Tóth, Entanglement detection, Physics Reports **474**, 1 (2009).
[67] G. Passetti, C. J. Eckhardt, M. A. Sentef, and D. M. Kennes, Cavity light-matter entanglement through quantum fluctuations, Phys. Rev. Lett. **131**, 023601 (2023).
[68] F. Schlawin, D. M. Kennes, and M. A. Sentef, Cavity quantum materials, Applied Physics Reviews **9**, 011312 (2022).
[69] I.-T. Lu, D. Shin, M. K. Svendsen, S. Latini, H. Hübener, M. Ruggenthaler, and A. Rubio, Cavity engineering of solid-state materials without external driving, Adv. Opt. Photon. **17**, 441 (2025).
[70] Q. Miao and G. S. Agarwal, Polaritonic ultrastrong coupling: Quantum entanglement in the ground state, Phys. Rev. Res. **5**, 033136 (2023).
[71] Y.-q. Liu, S. Sun, Y.-j. Yang, Z. Liu, X. Zhao, Z. Zhu, W. Liu, and C.-s. Yu, Quantum entanglement and einstein-podolsky-rosen steering in ultrastrongly light-matter-coupled systems, Phys. Rev. A **111**, 052437 (2025).
[72] N. C. Menicucci, S. T. Flammia, and O. Pfister, One-way quantum computing in the optical frequency comb, Phys. Rev. Lett. **101**, 130501 (2008).
[73] N. C. Menicucci, S. T. Flammia, H. Zaidi, and O. Pfister, Ultracompact generation of continuous-variable cluster states, Phys. Rev. A **76**, 010302(R) (2007).
[74] P. Roushan, C. Neill, A. Megrant, *et al.*, Chiral ground-state currents of interacting photons in a synthetic magnetic field, Nature Physics **13**, 146 (2017).
[75] A. Dareau, Y. Meng, P. Schneeweiss, and A. Rauschenbeutel, Observation of ultrastrong spin-motion coupling for cold atoms in optical microtraps, Phys. Rev. Lett. **121**, 253603 (2018).
[76] D. M. Meekhof, C. Monroe, B. E. King, W. M. Itano, and D. J. Wineland, Generation of nonclassical motional states of a trapped atom, Phys. Rev. Lett. **76**, 1796 (1996).
[77] B. Vermersch, T. Ramos, P. Hauke, and P. Zoller, Implementation of chiral quantum optics with rydberg and trapped-ion setups, Phys. Rev. A **93**, 063830 (2016).

Supplementary Files

This is a list of supplementary files associated with this preprint. Click to download.

- SupplementaryInformation.pdf